Chemical Geology 640 (2023) 121747

Contents lists available at ScienceDirect

Chemical Geology

journal homepage: www.elsevier.com/locate/chemgeo

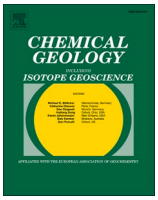

Interfacial adsorption of gold nanoparticles on arsenian pyrite: New insights for the transport and deposition of gold nanoparticles

Xin Nie [a], Quan Wan [a,b,*], Michael F. Hochella Jr [c,d], Suxing Luo [a,e], Meizhi Yang [a,e], Shanshan Li [f], Yuhong Fu [g], Ping Zeng [a,e], Zonghua Qin [a], Wenbin Yu [a]

[a] State Key Laboratory of Ore Deposit Geochemistry, Institute of Geochemistry, Chinese Academy of Sciences, Guiyang 550081, China
[b] CAS Center for Excellence in Comparative Planetology, Hefei 230026, China
[c] Department of Geosciences, Virginia Tech, Blacksburg, VA 24061, USA
[d] Division of Earth System Sciences, Pacific Northwest National Laboratory, Richland, WA 99354, USA
[e] University of Chinese Academy of Sciences, Beijing 100049, China
[f] School of Chemistry and Materials Science, Guizhou Normal University, Guiyang 550001, China
[g] School of Geographic and Environmental Sciences, Guizhou Normal University, Guiyang 550001, China

ARTICLE INFO

Editor: Oleg Pokrovsky

Keywords:
Gold nanoparticles
Arsenian pyrite
Adsorption
Surface properties
Solution chemistry
Negative charge-assisted hydrogen bonds

ABSTRACT

Gold nanoparticles (AuNPs) are found extensively in the near-surface Earth system. The transport, aggregation, and deposition of AuNPs have been potentially recognized as an important process and even a fundamental intermediary step both in formation of high-grade gold deposits and in the dispersion of gold into the Earth's surface environment. The interfacial adsorption between AuNPs and sulfide minerals is a long-recognized process regulating transport and deposition of gold in hydrothermal fluids, and the occurance of Au and As in pyrite are often observed in various hydrothermal Au deposits. However, the adsorption behavior of AuNPs on sulfide minerals and the fundamental chemical mechanism for the Au—As relationship remain enigmatic. In this work, we selected citrate as a surrogate for typical natural organic compounds abundantly found in lower-temperature hydrothermal systems and Earth's surface environment, and experimentally investigated the adsorption of negatively charged AuNPs on pyrite and arsenian pyrite under anaerobic conditions. We demonstrate that pyrite and nanoparticle surface properties, and solution chemistry, control the adsorption process. Negligible adsorption of AuNPs on pyrite (absent of As) was verified under all experimental conditions likely due to high electrostatic repulsion. However, we observed AuNPs adsorption on arsenian pyrite and suggest that this interaction is due to negative charge-assisted hydrogen bonds ((−)CAHBs) between hydroxyl/oxyl groups on the surface of arsenian pyrite and carboxyl groups on the citrate capping agent of AuNPs. Also, the lower negative charge density of arsenian pyrite surfaces significantly reduces electrostatic repulsion between both negatively charged AuNPs and arsenian pyrite. The solution pH, coexisting organics (citrate) concentration, and ionic strength are demonstrated to play substantial roles in the adsorption of AuNPs on arsenian pyrite. However, the solution pH appears to be an overriding factor controlling the adsorption of AuNPs which decreases with the increase of pH. With respect to citrate concentration, the adsorption rates of AuNPs onto arsenian pyrite initially decreases, but only slightly, and then increases. Increased ionic strength also promotes the adsorption of AuNPs. Our findings highlight a potentially important role of AuNPs in transport and deposition processes of gold in aqueous mediums, and provide new insights on the geochemical behavior of metal nanoparticles in the hydrothermal systems and Earth's surface environment.

1. Introduction

Metal nanoparticles have been found extensively in various portions of the Earth system, including the atmosphere, hydrosphere (e.g. oceans, lakes and rivers, ground-water, and hydrothermal vents), lithosphere, and biosphere (Hochella et al., 2019; Sharma et al., 2015). The continuing increase in production and use of gold nanoparticles (AuNPs) in a wide range of consumer products and their direct or indirect

* Corresponding author at: State Key Laboratory of Ore Deposit Geochemistry, Institute of Geochemistry, Chinese Academy of Sciences, Guiyang 550081, China.
E-mail address: wanquan@vip.gyig.ac.cn (Q. Wan).

https://doi.org/10.1016/j.chemgeo.2023.121747
Received 1 August 2023; Received in revised form 14 September 2023; Accepted 22 September 2023
Available online 23 September 2023
0009-2541/© 2023 Elsevier B.V. All rights reserved.

applications inevitably result in their release into the environment. AuNPs could not only influence the transport and fate of harmful heavy metals, metalloids, radionuclides and organic pollutants in the Earth's surface environment, but also change the bioavailability, toxicity, and geochemical cycling of contaminants as well as nanoparticles in the environment, and consequently might have a potentially deleterious impact on human and environmental health (Hochella et al., 2019; Miller et al., 2017; Sharma et al., 2015). In addition, naturally formed AuNPs (or colloidal gold particles) have been increasingly recognized as an important component of gold in various geological environments (e.g., hydrothermal fluids, black smoker fluids, hydrothermal deposits, and supergene enrichments) (Gartman et al., 2017; Hannington and Garbe-Schonberg, 2019; Hough et al., 2011; McLeish et al., 2021; Petrella et al., 2022; Xian et al., 2022). A variety of mechanisms, including chemical, physical, and biological processes separately or in combination, have been proposed to explain the occurrence of AuNPs in hydrothermal fluids and Earth surface environments (Gartman et al., 2019; Hannington et al., 2016; McLeish et al., 2021; Petrella et al., 2020; Reich et al., 2011; Sharma et al., 2015). Previous studies have documented that the formation, transport, aggregation, and deposition of AuNPs have been potentially recognized as an important process and even a fundamental intermediary step both in formation of high-grade gold deposits and in the dispersion of gold into the environment (Hastie et al., 2021; Lee et al., 2021; Saunders, 1990; Saunders et al., 2020). When AuNPs are present in hydrothermal and supergene environments, they will be inevitably subject to interaction with various minerals (Hochella et al., 2019). The adsorption and deposition of AuNPs on minerals has been found to be a critical interfacial interaction process in governing their geochemical reactions, and the migration and fate of gold in the hydrothermal systems and Earth surface environments (Becker et al., 2010; Sharma et al., 2015; Uchimiya et al., 2017; Zhou et al., 2021). However, the underlying mechanism of interfacial adsorption and deposition of AuNPs on minerals remains unclear. Therefore, a better understanding of the geochemical behaviors of AuNPs in an aqueous medium requires detailed experimental studies.

Pyrite and arsenian pyrite are the common gold-bearing sulfide minerals in many hydrothermal gold ore deposits and widely exist in Earth surface environments (Thiel et al., 2019). Previous studies have documented coupled geochemistry of Au and As in sulfides from hydrothermal ore deposits, suggesting that arsenic might play a crucial role during the enrichment process of Au, in which the incorporation of As into the pyrite structure is likely to enhance the adsorption and deposition of Au-sulfide complexes and AuNPs on pyrite surfaces (Deditius et al., 2014; Gopon et al., 2019; Kusebauch et al., 2019; Large et al., 2009; Pokrovski et al., 2021; Reich et al., 2005). Previous studies have investigated the adsorption of AuNPs on pyrite, but these works focused primarily on oxidized and natural pyrite surfaces (Fu et al., 2017; Luo et al., 2018; Mikhlin et al., 2011). Such pyrite commonly contains a variety of surface oxidation products and various trace elements, which would result in variations of surface reactivity at nanoscale, and consequently significantly affect the adsorption of AuNPs (Fu et al., 2017; Murphy and Strongin, 2009; Zhu et al., 2018). To date, experimental studies focusing on interfacial interaction between AuNPs and arsenian pyrite under anaerobic condition are limited, although understanding such interactions are critical in developing microscopic mechanisms for these processes.

Therefore, an experimental study on the adsorption of AuNPs on synthetic pyrite and arsenian pyrite surface was carried out under anaerobic conditions and in the presence of a representative organic compound. It is worth noting that abundant organic matter has been found in in various geological environments (e.g., supergene environments and hydrothermal ore deposits) (Lee et al., 2021; Migdisov et al., 2017; Sharma et al., 2015). Organic matter may significantly contribute to the formation of AuNPs via the reduction of aqueous gold species in the aquatic environment (Lee et al., 2021; Williams-Jones et al., 2009). These ubiquitous natural organic molecules commonly contains hydroxyl and carboxyl groups that can also readily cap and stabilize AuNPs, and consequently may contribute to the transport of AuNPs in aqueous suspension (Crede et al., 2019; Hotze et al., 2010; Sharma et al., 2015; Williams-Jones et al., 2009). Thus, in this work, citrate, which contains both hydroxyl and carboxyl groups, was selected as a reasonable surrogate for natural organics (e.g. humic substances) to experimentally investigate its role in the geochemical behavior of AuNPs (Liu et al., 2019). The effects of arsenic incorporation into pyrite lattice and various solution conditions, including solution pH, the concentration of ligand (citrate), and ionic strength, were systematically investigated to evaluate the roles of these factors in the adsorption behavior of AuNPs. Finally, a possible adsorption mechanism, and geochemical implications are also discussed.

2. Methods

2.1. Synthesis of arsenian pyrite

Arsenian pyrite with arsenic content of 2.5 wt% was prepared using a hydrothermal method (Luo et al., 2018). Deoxygenated deionized water was used in all experiments. In a typical process, 0.015 mol of $FeSO_4{\cdot}7H_2O$, 0.015 mol of $Na_2S{\cdot}9H_2O$, and arsenic powder (0.001 mol) were first mixed in 40 mL of water at room temperature and a black suspension appeared immediately. Then 0.015 mol of $Na_2S{\cdot}9H_2O$ and 0.015 mol of S were mixed into 20 mL of water and heated until the solution became transparent, which was subsequently added dropwise to the above black suspension under vigorous stirring for 10 min. The suspension was then transferred into a 100 mL Teflon-line autoclave, and then hydrothermally treated at 200 °C in an oven for 24 h. After the hydrothermal reaction, the product was collected by centrifugation, and thoroughly washed with 1 mol/L H_2SO_4, 1 mol/L of Na_2S boiling solution, water, and absolute ethanol for several times. Finally, the as-synthesized black sample was dried at 40 °C for 6 h in a vacuum oven (DZF-6050, Shanghai Shenxian Thermostatic Equipment, China) and then stored in a glove box in an anaerobic environment. For comparison, pure pyrite (absent of As) was prepared without adding arsenic powder under the same experimental conditions.

2.2. Adsorption experiments

Spherical AuNPs with an average diameter of about 18 nm were synthesized according to our previous work (Fu et al., 2017; Luo et al., 2018). In a typical synthesis procedure, 17.5 mL of sodium citrate solution (1.00%, w/w) was quickly added to 500 mL of boiling $HAuCl_4$ solution (0.01%, w/w) and stirred at 100 °C for 30 min. The resulting samples were cooled down to ambient temperature and stored in a refrigerator at 4 °C. All adsorption experiments were performed in an anaerobic glove box at room temperature. The concentration of dissolved oxygen in the suspensions was determined to be <0.1 ppm using a dissolved oxygen meter (JPB-607 A). The reaction solution was kept at approximately 25 °C and stirred with a magnetic stirrer throughout the experiment. In a typical adsorption experiment, 0.04 g of fresh arsenian pyrites or pyrite was first added into 32 mL of 58 ppm Au colloid in a 40-mL sealed glass bottle with an initial pH of 4.0–7.4 $\pm$ 0.05 adjusted by adding HCl or NaOH. Then, at different time intervals, the pHs of suspensions were measured, and 2.5 mL of suspension was collected and centrifuged for 5 min (4000 rcf) for later analysis. Afterward, an aliquot (1.5 mL) of the resulting supernatant was digested overnight with 1 mL of aqua regia to analyze the Au concentration using flame Atomic Absorption Spectroscopy (AAS, 990SUPER, Persee, China; detection limit 0.1 ppm). The concentration of dissolved iron in the supernatant was also measured by AAS. The extent of adsorption was determined based on the difference in Au concentration between initial and final liquid phases. Citrate concentrations were determined using high-performance liquid chromatography (HPLC, Agilent 1200, USA) equipped with a dual absorbance detector (DAD) at a wavelength of 215 nm and a Zorbax SB-

aq (3 × 100 mm, 1.8 μm) (Agilent) C18 reverse phase column. The mobile phase was a H_3PO_4 solution (0.1%, v/v) with a flow rate of 0.6 mL/min. The resulting solid products through centrifugation were dried and finally observed using scanning electron microscopy (SEM, Scios, FEI Company, USA) with an acceleration voltage of 30.0 kV. The chemical composition and chemical species of the surface of arsenian pyrite and pyrite after adsorbed AuNPs were characterized by X-ray photoelectron spectroscopy (XPS, Thermo Fisher K-Alpha, USA), attenuated total reflectance-Fourier transform infrared (ATR-FTIR, Bruker Vertex 70 spectrometer, Germany), and Micro-Raman Spectrometry.

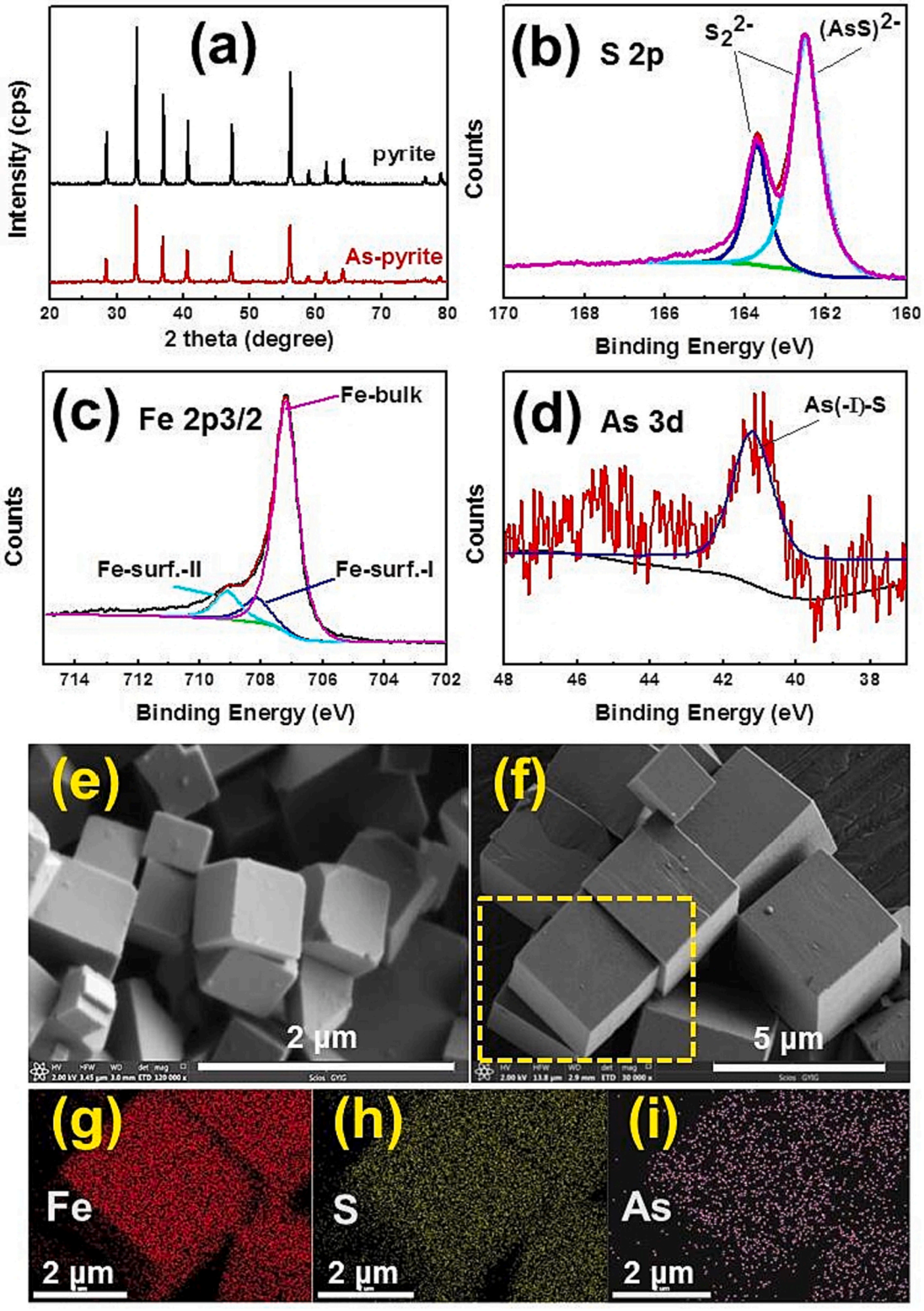

Fig. 1. XRD patterns (a) of as-synthesized pure pyrite and arsenian pyrite; XPS spectra of arsenian pyrite (b, c, and d); SEM images of pure pyrite (e) and arsenian pyrite (f); EDS elemental mapping of arsenian pyrite cubic micro-particles (g–i).

3. Results

3.1. Characterization of as-prepared pyrite and arsenian pyrite

Fig. 1a shows the powder X-ray diffraction (XRD) patterns of the as-synthesized pure pyrite and arsenian pyrite (As-pyrite). Pyrite was found to be the only crystalline phase in both samples. The diffraction peaks at $2\theta = 28.51°$, 33.08°, 37.11°, 40.78°, 47.41°, 56.28°, 59.02°, 61.69°, and 64.28° were well attributed to the (111), (200), (210), (211), (220), (311), (222), (023), and (321) planes of cubic pyrite (FeS_2) (JCPDS card no. 42–1340) with a space group of $Pa\bar{3}$, respectively (Nie et al., 2022). Compared with pure FeS_2, no peak shifts of arsenian pyrite could be observed, indicating no phase change after a small amount of As doping. The characteristic diffraction peaks are sharp, suggesting good crystallinity of both pure pyrite and arsenian pyrite. However, the intensity of the XRD peaks of arsenian pyrite were found to be weaker than that of pure pyrite due to the substitution of S by As favors the formation of sulfur vacancies and distortion of the pyrite structure (Abraitis et al., 2004; Blanchard et al., 2007; Deditius et al., 2008). The Raman spectra of pure pyrite and arsenian pyrite (Fig. S1) display three peaks at 340, 372, and 423 cm^{-1}, which represent the Fe—S liberational motion (Eg), Fe—S stretching motion (Ag) and S—S stretching motion (Tg) modes of pyrite crystals, respectively (Wen et al., 2015). No other obvious feature of vibrational peaks of iron sulfides and oxides could be observed, implying once again that pyrite is the sole phase for both pyrite and arsenian pyrite samples (Gong et al., 2013).

Fig. 1b, c, and d, illustrate the X-ray photoelectron spectroscopy (XPS) of arsenian pyrite. The surface of arsenian pyrite is composed of the elements S (about 50 wt% or 65 at.%), Fe (about 46 wt% or 33 at.%), and a small amount of As (about 2.5 wt% or 1.5 at.%). The S 2p bands can be fitted with the doublets at binding energies of 162.4 and 163.6 eV, which corresponds to polysulfide species (S_2^{2-}) in pyrite or $(AsS)^{2-}$ anions in arsenian pyrite (Blanchard et al., 2007; Mikhlin et al., 2006). The Fe $2p_{3/2}$ peak at 707.2 eV is assigned to low spin bulk Fe^{2+} in pyrite.

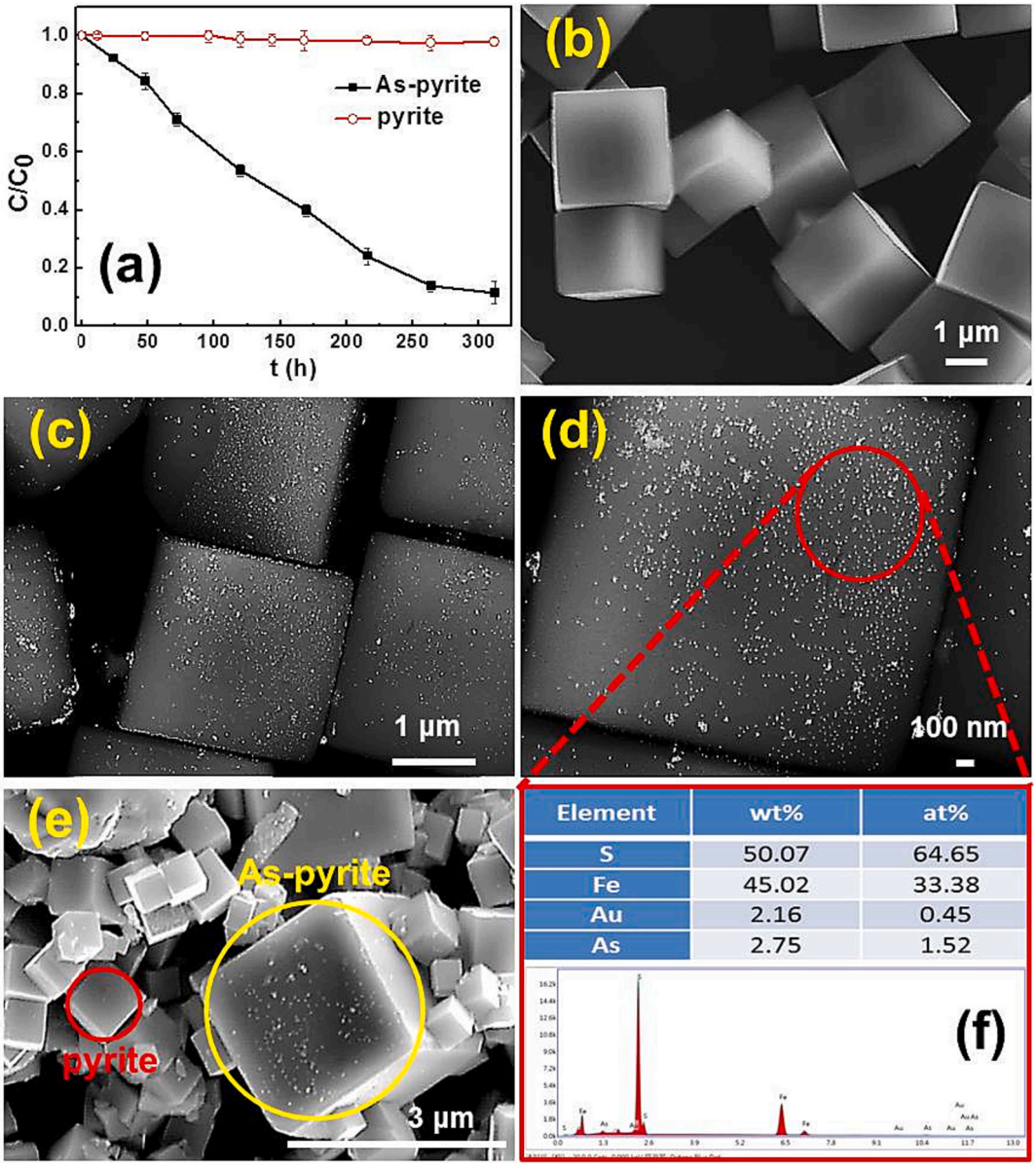

Fig. 2. (a) Adsorption curves of AuNPs (the initial concentration was 58 ppm) on pure pyrite or arsenian pyrite at pH 4.0 under anoxic condition; SEM images of arsenian pyrite before (b) and after (c and d) adsorption of AuNPs at pH 4.0 after 312 h stirring under anoxic condition; (e) SEM image of the mixture of pure pyrite and arsenian pyrite after adsorption of AuNPs for 312 h at pH 4.0; EDX analysis (f) of arsenian pyrite recorded from the red circled area of Fig. 2d. (For interpretation of the references to colour in this figure legend, the reader is referred to the web version of this article.)

The other two peaks centered at 708 and 709 eV are attributed to two Fe surface states of Fe-surf.-I and Fe-surf.-II, respectively (Nesbitt et al., 1998; Zhu et al., 2018). The As 3d peak at 41.2 eV reveals an oxidation state of As^{1-} for the synthetic arsenian pyrite samples, which suggests incorporation of arsenic within the pyrite lattice forming $(AsS)^{2-}$ dianion groups by substituting for tetrahedral sulfur (Blanchard et al., 2007; Le Pape et al., 2017; Mikhlin et al., 2006; Qiu et al., 2018).

The morphology of the pure pyrite and arsenian pyrite samples was characterized by SEM (Fig. 1e–i). Fig. 1e shows the typical cubic shape of pure pyrite particles with a size of ca.500–700 nm. For arsenian pyrite (Fig. 1f), the size of the cubic particles ranged from 1.5 to 4 μm, suggesting that the As^{1-} incorporation into FeS_2 may be beneficial to crystal growth (Le Pape et al., 2017). The specific surface areas of pure pyrite and arsenian pyrite were measured to be ~5 and ~ 0.8 m^2/g, respectively, qualitatively in accordance with their particle sizes. Fig. 1g–i show the Energy dispersive spectroscopy (EDS) elemental mapping analysis recorded from the yellow squared area in Fig. 1f. The EDS results confirm the element composition of arsenian pyrite (S/Fe ~2, As 2.4–2.8 wt%) consistent with the XPS spectra.

3.2. Adsorption of AuNPs on pure pyrite and arsenian pyrite

Fig. 2a shows the adsorption curves of AuNPs in a suspension containing pure pyrite or arsenian pyrite at pH 4.0 under anoxic condition. Apparently, Au concentration in the liquid phase remained almost unchanged within 312 h in the presence of pure pyrite, indicating negligible adsorption of AuNPs on the pure pyrite surface. Additional adsorption experiments of AuNPs by pure pyrite (Fig. S2) under extended pH range (4.0–7.4) further demonstrated that AuNPs could not be adsorbed by pure pyrite regardless of the pH values. In contrast, when mixing AuNPs with arsenian pyrite in a suspension at pH 4.0, Au concentration in the liquid phase gradually decreased with the stirring time. The residual Au concentration in the liquid phase at 264 h became approximately 13% compared with initial AuNPs colloids, indicating that ~87% of AuNPs were adsorbed by the arsenian pyrite. Further increasing the stirring time to 312 h did not significantly lower the residual Au concentration in the liquid phase (~10%). The adsorption data within 264 h follows the pseudo-zeroth-order kinetics ($C_0 - C = 0.0035$ t) with a high regression coefficient R^2 value (0.9903). Fig. 2b-d shows the SEM images of arsenian pyrite before and after adsorption with AuNPs at pH 4.0. The surface of the cubic arsenian pyrite particles appears quite smooth and clean before the adsorption of AuNPs (Fig. 2b), while a large number of AuNPs are clearly observed on the surface of arsenian pyrite after adsorption (Fig. 2c and d). EDS analysis (Fig. 2f) confirms the presence of Au on arsenian pyrite, which also indicates that the molar ratio of S/Fe/As remained nearly unchanged before and after adsorption with AuNPs.

To further test whether AuNPs could be preferentially adsorbed on arsenian pyrite instead of pure pyrite, an adsorption experiment in a suspension containing both pure pyrite and arsenian pyrite with equivalent mass was also carried out. Approximately 50% AuNPs were adsorbed within 312 h. Fig. 2e shows the SEM image of the mixture of pure pyrite and arsenian pyrite after adsorption of AuNPs within 312 h at pH 4.0. Similar to the abovementioned results, no obvious AuNPs could be found on the surface of pure pyrite having a smaller size of ca.500–700 nm. Nevertheless, a large number of Au nanoparticles were observed on the surface of arsenian pyrite having a larger size of 1.5–4 μm. The result confirms that AuNPs would be preferentially adsorbed on the arsenian pyrite surface rather than pure pyrite, indicating that the incorporation of arsenic into pyrite facilitates the adsorption of AuNPs. It should be noted that the specific surface area of pure pyrite is 6–7 times higher than arsenian pyrite, negligible adsorption of AuNPs on pure pyrite surface and significant adsorption of AuNPs on arsenian pyrite surface were observed. Therefore, this means that the differences in specific surface areas of pure pyrite and arsenian pyrite should not be the dominant factor controlling adsorption of AuNPs.

The surface chemical composition and chemical state of the arsenian pyrite after adsorption of AuNPs for 312 h were characterized by XPS (Fig. S3). As shown, the sample is mainly composed of the elements S (Fig. S3A), Fe (Fig. S3B), and a small amount of As (Fig. S3C) and Au (Fig. S3D). Compared with the spectra of arsenian pyrite before adsorption of AuNPs (Fig. 1b-d), no detectable changes of oxidation state and relative content for S, Fe and As could be observed, confirming that there is no oxidation of the arsenian pyrite surface during the adsorption process of AuNPs. Supplemental Fig. S3D shows the characteristic XPS spectrum of metallic gold (Au $4f_{7/2}$ binding energy at 84.1 eV), indicating that AuNPs was successfully adsorbed onto the surface of arsenian pyrite.

3.3. Effect of initial suspension pH on AuNPs adsorption on arsenian pyrite

The effect of pH on the adsorption behavior of AuNPs on the arsenian pyrite surface was systematically investigated (Fig. 3). Fig. 3a shows the adsorption curves of AuNPs on arsenian pyrite at different initial pH values. Clearly, adsorption of AuNPs was highly pH dependent, with adsorption efficiency steadily decreasing with increasing initial suspension pH from 4.0 to 7.4 (data below pH 4.0 not considered due to apparent homoaggregation of AuNPs). For instance, approximately 90%, 65%, and 4% of AuNPs were adsorbed after 312 h of stirring at an initial pH of 4.0, 5.0, and 6.0, respectively. However, Au concentration in the supernatant remained almost unchanged within 312 h when the initial pH exceeded 7.4. SEM images of arsenian pyrite after adsorption with AuNPs at different initial pHs with the stirring time of 312 h are given in Fig. 3 d-e. At pH 4.0, numerous AuNPs could be observed on the arsenian pyrite surface after 312 h of adsorption (Fig. 3d), while the number of adsorbed AuNPs became remarkably reduced when the initial suspension pH was increased to 5.0 (Fig. 3e). When the initial pH of suspensions was further increased to 6.0, almost no AuNPs could be observed on the surface of arsenian pyrite (Fig. 3f).

The pH values of the above adsorption suspensions with different initial pHs are presented in Fig. 3b, which indicates that the suspension pH gradually increased with the stirring time regardless of the initial pHs. Specifically, the pH of the suspension with an initial pH of 4.0, 5.0, 6.0, and 7.4 rose to 4.61, 5.87, 7.41, and 8.32 at 312 h, respectively, suggesting the release of OH^- or consumption of H^+ during the adsorption process. Because citrate functioned as both a reducing and stabilizing agent when synthesizing AuNPs, it should be noted that a considerable amount of citrate (~1 mM) remained in the final gold colloids as well as the adsorption suspensions. Hence, for comparison, arsenian pyrite was also mixed with water in the absence of citrate and AuNPs, and the corresponding pH variations of suspensions with different initial pHs are shown in Fig. 3c. A similar ascending trend of the pH variation with stirring time was observed for suspensions without citrate and AuNPs. Interestingly, the pH values of suspensions without citrate (especially those with low initial pHs, e.g., 4.0 and 5.0) increased more significantly compared with suspensions containing 1 mM citrate, reaching ~7.38, 7.44, 7.42, and 8.40 at 312 h for suspensions with initial pH 4.0, 5.0, 6.0, and 7.4, respectively.

3.4. Effect of citrate concentration on the adsorption behavior of AuNPs on arsenian pyrite

The effect of organics on the adsorption behavior of AuNPs on arsenian pyrite were investigated with different concentrations of citrate. Fig. 4a shows the adsorption curves of AuNPs on arsenian pyrite at different citrate concentrations at initial pH 4.0. When the citrate concentration increased from 1 to 2 mM, the adsorption rate of AuNPs slightly decreased and the adsorption efficiency of AuNPs at 312 h also decreased from 90% to 87%. On the other hand, when further increasing the citrate concentration to 5 and 7.5 mM, the adsorption rate of AuNPs greatly increased. For the suspension with 5 mM citrate, approximately

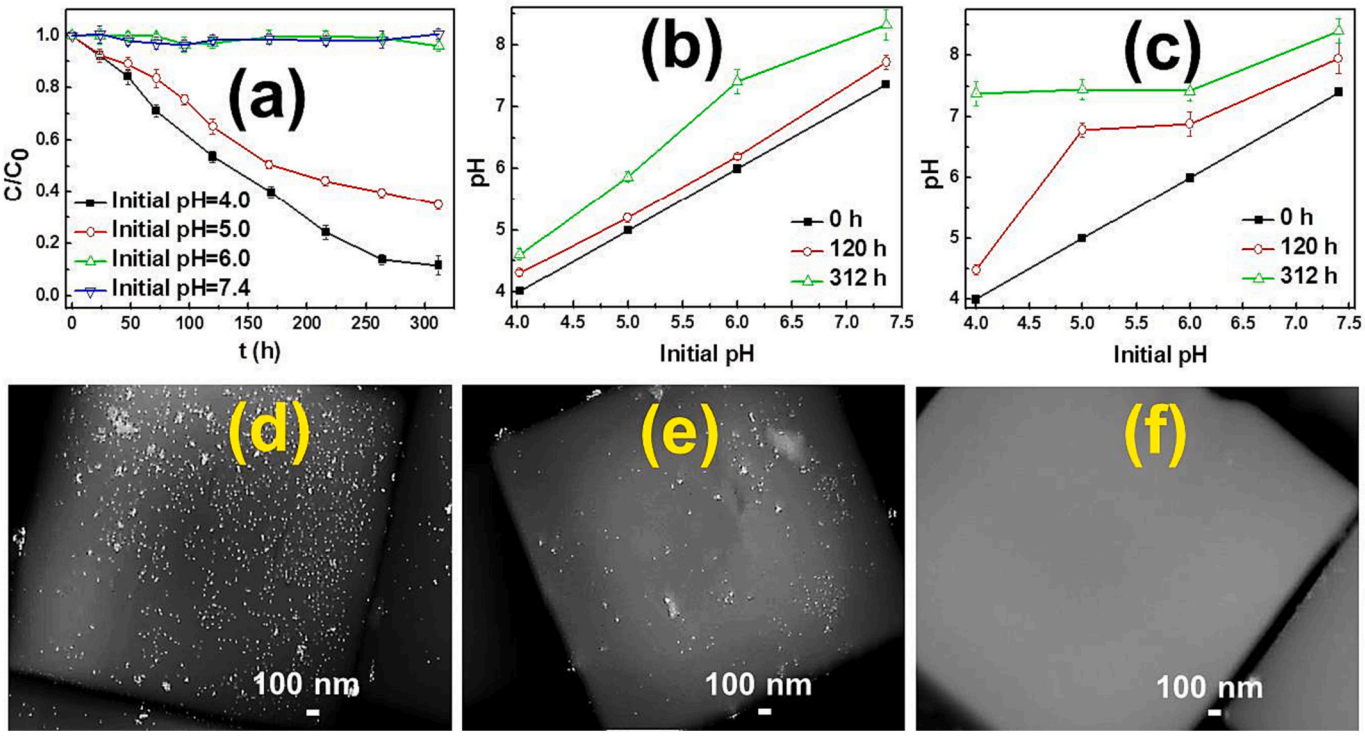

Fig. 3. (a) Adsorption curves of AuNPs on arsenian pyrite at different initial pH values; changes of the suspension pH with different initial pHs and stirring times during adsorption process of AuNPs (b) and in pure water without AuNPs (c); SEM images of arsenian pyrite after adsorption of AuNPs at different initial pHs after stirring for 312 h: (d) pH 4.0; (e) pH 5.0; (f) pH 6.0.

98% of AuNPs were adsorbed onto arsenian pyrite after 312 h of stirring. In the presence of 7.5 mM citrate, an almost thorough adsorption of AuNPs could be reached only after 170 h. Because homoaggregation of AuNPs could be obviously observed when the citrate concentration reached 10 mM, adsorption experiments with citrate concentration above 7.5 mM was not conducted. SEM images of arsenian pyrite after 312 h stirring with AuNPs in the presence of different citrate concentrations demonstrates substantial adsorption of AuNPs (Fig. 4c-f). Consistent with the measurements in Fig. 4a, the amount of adsorbed AuNPs appears to slightly decrease with the increase of citrate concentration from 1 to 2 mM (Fig. 4c and d), which however increased significantly with the citrate concentration further increased to 5 (Fig. 4e) and 7.5 mM (Fig. 4f).

Fig. 4b illustrates the changes of suspension pH at different initial citrate concentrations. The pHs of all suspensions gradually increased with the stirring time. Nevertheless, the magnitude of pH change dramatically decreased with the increase of citrate concentration. With the same initial pH of 4.0, the suspension pH at 312 h was 4.61, 4.17, 4.10, and 4.03 for citrate concentration of 1, 2, 5, and 7.5 mM, respectively, implying a higher pH buffering effect with a higher citrate concentration.

3.5. *Effect of ionic strength on the adsorption behavior of AuNPs on arsenian pyrite*

The influence of ionic strength on the adsorption of AuNPs on arsenian pyrite was studied by adding different concentrations of NaCl. Fig. 5a illustrates the adsorption curves of AuNPs on arsenian pyrite at initial pH 4.0 and with different NaCl concentrations. The adsorption rate of AuNPs without the addition of NaCl was slower than that in the presence of additional NaCl. When the concentration of added NaCl increased from 0 to 10 mM, the adsorption efficiency of AuNPs at 312 h increased from 90 to 96%. Fig. 5c-e show SEM images of arsenian pyrite after 312 h adsorption with AuNPs at initial pH 4.0 and different NaCl concentrations. Based on SEM observation, the particle size of the adsorbed AuNPs increased significantly with the addition NaCl, suggesting that the increase of ionic strength may promote the agglomeration of AuNPs adsorbed onto arsenian pyrite. The pH changes during the adsorption processes within the suspensions at an initial pH of 4.0 and with the addition of different concentrations of NaCl is shown in Fig. 5b, which shows again that the suspension pH gradually increased with the stirring times.

4. Discussion

4.1. *Surface charge properties of AuNPs, pyrite, and arsenian pyrite*

To understand the surface charge characteristics of AuNPs, arsenian pyrite and pure pyrite, their zeta potentials were measured. Fig. 6a illustrates the zeta potential values of AuNPs, arsenian pyrite and pure pyrite in the absence or presence of citrate at different pHs. The zeta potential values of AuNPs were negative in the pH range of 2.8–10.1, indicating that AuNPs are negatively charged at all tested pH conditions. The zeta potential became increasingly more negative with increasing pH from 2.8 to 7.0, suggesting a higher surface negative charge density of AuNPs at higher pH. When the pH exceeds 7.0, the zeta potential began to become less negative. However, the relative high negative values of the zeta potential (<-20 mV) in the pH range of 4.0–10.1 further confirm the reasonable dispersion stability of AuNPs in solution. As a commonly used reductant to synthesize and stabilize AuNPs, citrate will bind to surface gold atoms via central carboxyl groups to form covalent Au—O bonds (Al-Johani et al., 2017; Park and Shumaker-Parry, 2014; Sharma et al., 2014). Fig. S4 shows the relative abundances of citric acid species in aqueous solution at different pHs. Citric acid is a triprotic acid ($pK_{a1} = 3.13$, $pK_{a2} = 4.76$ and $pK_{a3} = 6.40$), thus the deprotonation of citric acid increases with increasing the pH, and consequently, the surface charge as well as the zeta potential of AuNPs became generally more negative at higher pH (Beck, 1977; Luo et al.,

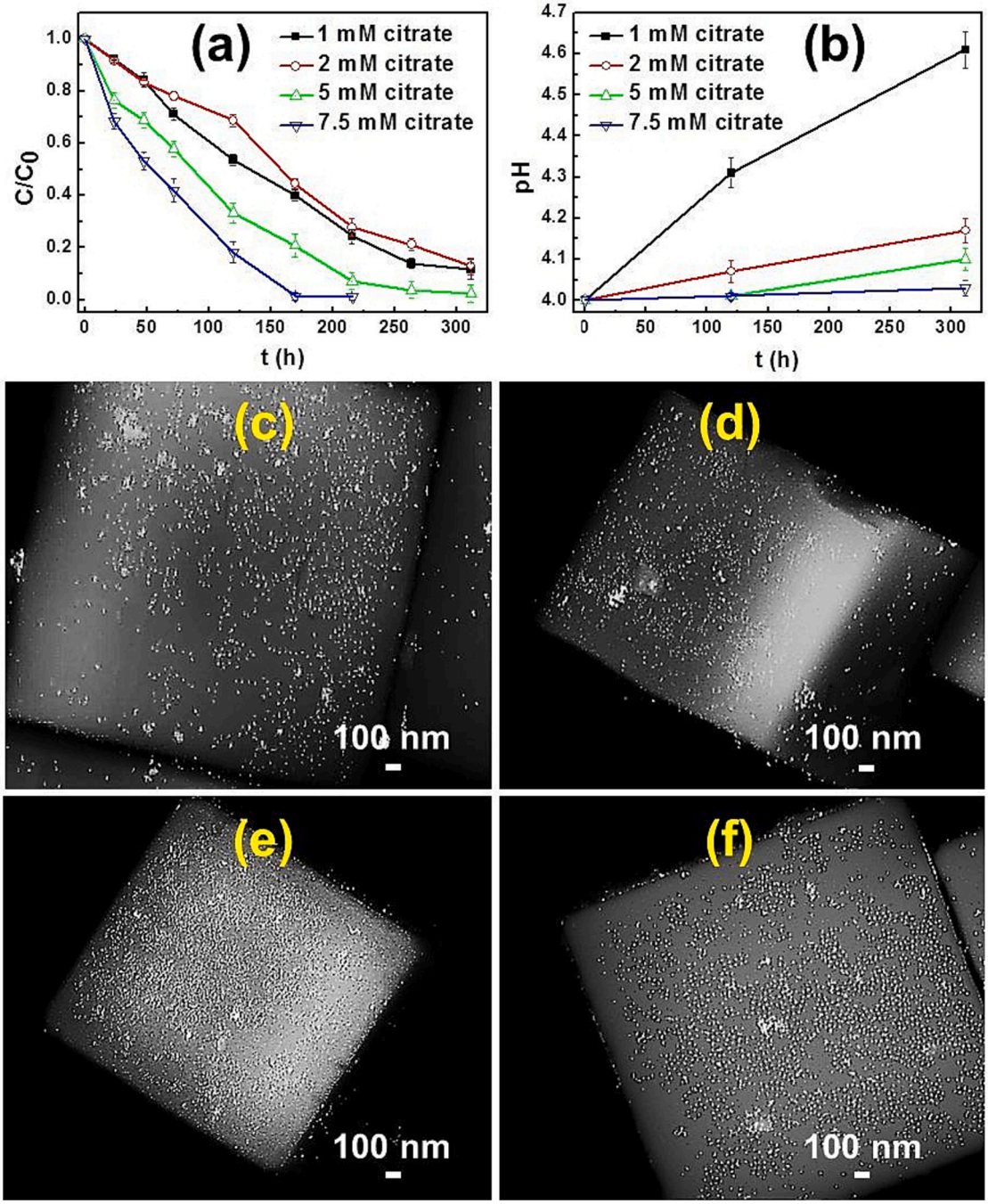

Fig. 4. Adsorption curves of AuNPs on arsenian pyrite at different citrate concentrations at initial pH 4.0 (a) and changes of the suspension pH at different initial citrate concentrations (b); SEM images of arsenian pyrite after 312 h adsorption with AuNPs at initial pH 4.0 and different concentrations of citrate: (c) 1 mM; (d) 2 mM; (e) 5 mM; (f) 7.5 mM.

2018). However, under alkaline conditions, the electrostatic repulsion between neighboring highly deprotonated citrate (obtaining a 3-charge) would reduce the surface coverage of citrate on the surface of AuNPs, and consequently reduce the surface charge density and the absolute value of the zeta potential of AuNPs (Luo et al., 2018; Park and Shumaker-Parry, 2015).

The zeta potential values of both arsenian pyrite and pure pyrite are also dependent on the solution pH, and the isoelectric point (pH_{iep}) of arsenian pyrite and pure pyrite in the absence of citrate is ~pH 2.2 and pH 1.5, respectively. Thus, both arsenian pyrite and pure pyrite are negatively charged within the pH range of our adsorption experiment due to the presence of various types of dissociable groups, including ≡S–H, ≡S–OH, and ≡Fe–OH on the pyrite surface, which would be protonated to generate positive charge at pH < pH_{iep} and deprotonated to yield negatively charged surface sites at pH > pH_{iep} (Bebie et al., 1998; Weerasooriya and Tobschall, 2005). A lower atomic electronegativity for elemental arsenic (5.3 eV) than sulfur (6.22 eV) at the mineral surface seems to make arsenian pyrite have a higher pH_{iep} value than pure pyrite (Bebie et al., 1998). Furthermore, the zeta potential of pure pyrite was more significantly negative than arsenian pyrite in pure water without citrate at pH > 2.2, suggesting that the pure pyrite surface possesses more negative charges than arsenian pyrite. This is likely due to a lower atomic proportion of sulfur on arsenian pyrite surface, which decreases the density of amphoteric surface groups such as ≡S–H and

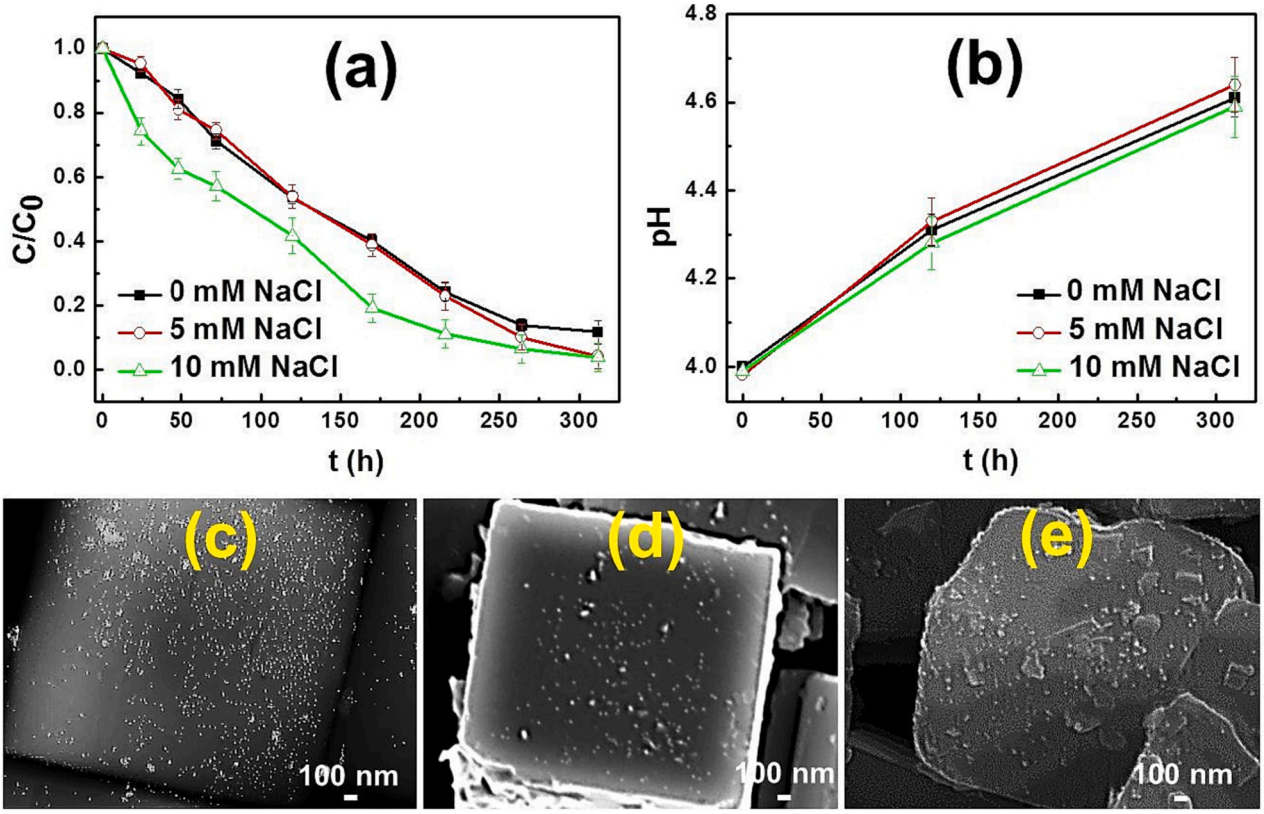

Fig. 5. Adsorption curves of AuNPs on arsenian pyrite (a) and changes of the suspension pH (b) at initial pH 4.0 and with different NaCl concentrations; SEM images of arsenian pyrite after 312 h adsorption with AuNPs at initial pH 4.0 and different NaCl concentrations: (c) 0 mM; (d) 5 mM; (e) 10 mM.

≡S–OH, and consequently reduces negative charge density of arsenian pyrite compared to pure pyrite. This suggests that the sulfur surface groups are the dominant surface functional groups and govern the surface chemical and electrokinetic properties of pure pyrite and arsenian pyrite to a large extent (Bebie et al., 1998).

Compared with the pure water systems, there were only minor differences in the pH_{iep} values for both arsenian pyrite and pure pyrite upon the addition of citrate. Only subtle differences in the zeta potential values of pure pyrite in the absence and presence of citrate could be observed from pH 2 to 11, suggesting that citrate may not interact with the pure pyrite surface. However, the addition of citrate into the arsenian pyrite suspension significantly increased the values of negative surface potentials compared to the citrate-free system, and the zeta potential dramatically became more negative with an increase of the suspension pH. For instance, the zeta potential of arsenian pyrite increased in magnitude from −7.5 mV in pure water to −21.5 mV in 1 mM citrate at pH 3.0 and from −18.0 mV in pure water to −79.0 mV in 1 mM citrate at pH 7.5. This suggests that citrate could intimately interact with the surface groups of arsenian pyrite unlike pure pyrite. With increasing the suspension pH, the dissociation of citric acid and its negative charge increases, the zeta potential dramatically became more negative. At pH over 7.5, the absolute value of the zeta potential reached a plateau due to nearly complete dissociation of citric acid (Luo et al., 2018). However, the HPLC chromatograms (Supplemental Figs. S5 and S6) of the supernatants obtained from the suspensions containing arsenian pyrite and 1 mM citrate at different reaction intervals under different pHs did not show an obvious decrease in citrate concentration because of the relatively low specific surface area of arsenian pyrite (Uchimiya et al., 2017).

To further validate the effects of solution conditions on the surface charge characteristics of arsenian pyrite and AuNPs during the adsorption processes, the variations of the zeta potential of arsenian pyrite and AuNPs were also measured at different stirring times at different conditions, including initial pH (Fig. 6b), concentrations of citrate (Fig. 6c), and ionic strengths (Fig. 6d). Fig. 6b shows the variations of zeta potentials of arsenian pyrite at different initial pHs in the presence of 1 mM citrate. The zeta potential of arsenian pyrite at initial pH 4.0, 5.0, and 6.0 was −29.15, −51.58, and − 68.26 mV, respectively, at 2 h, and then increased in magnitude to −45.33, −66.56, and − 79.57 mV at 312 h, respectively (Fig. 6b). This is ascribed to the increased solution pH (from 4.0, 5.0, and 6.0 to 4.61, 5.87, and 7.41, respectively) (Fig. 3b and c), which induces the zeta potential to become more negative. The increase of solution pH with stirring time may be related to the release of OH^- or proton assimilation originating from a surface complexation of H^+ onto arsenian pyrite during the dissolution process according to the following scheme: $\equiv FeS_2 + H^+ \rightarrow \equiv FeS_2{\cdot}H^+ \rightarrow \equiv Fe^{2+}HS_2 \rightarrow \equiv S_2H + Fe^{2+}$ (Weerasooriya and Tobschall, 2005). This speculation is further confirmed by the results of Fe^{2+} release into the solution (Supplemental Fig. S7), in which the increase of the concentration of dissolved Fe^{2+} is accompanied an increase in solution pH during the adsorption processes. At higher initial pH (e.g. 7.4), the zeta potential of arsenian pyrite showed no significant changes with increasing the stirring time, which is similar to the trend (as shown in Fig. 6a) that the zeta potential of arsenian pyrite reached a relatively constant value at a solution pH over 7.5.

Fig. 6c illustrates the variations of zeta potentials of AuNPs and arsenian pyrite as a function of citrate concentration at initial pH 4.0. As shown, increasing citrate concentration from 1 to 7.5 mM led to the zeta potential of AuNPs significantly becoming more negative from −20.8 to −34.8 mV due to an increased citrate surface coverage of AuNPs. However, with a stirring time of 2 h, the magnitude of the negative zeta potential of arsenian pyrite initially increased slightly from −29.15 to −31.77 mV with the citrate concentration increasing from 1 to 5 mM, and then remarkably decreased to −21.27 mV (7.5 mM citrate). This may be attributed to an increase of adsorbed citrate by arsenian pyrite as the citrate concentration increased in the solution which gives more

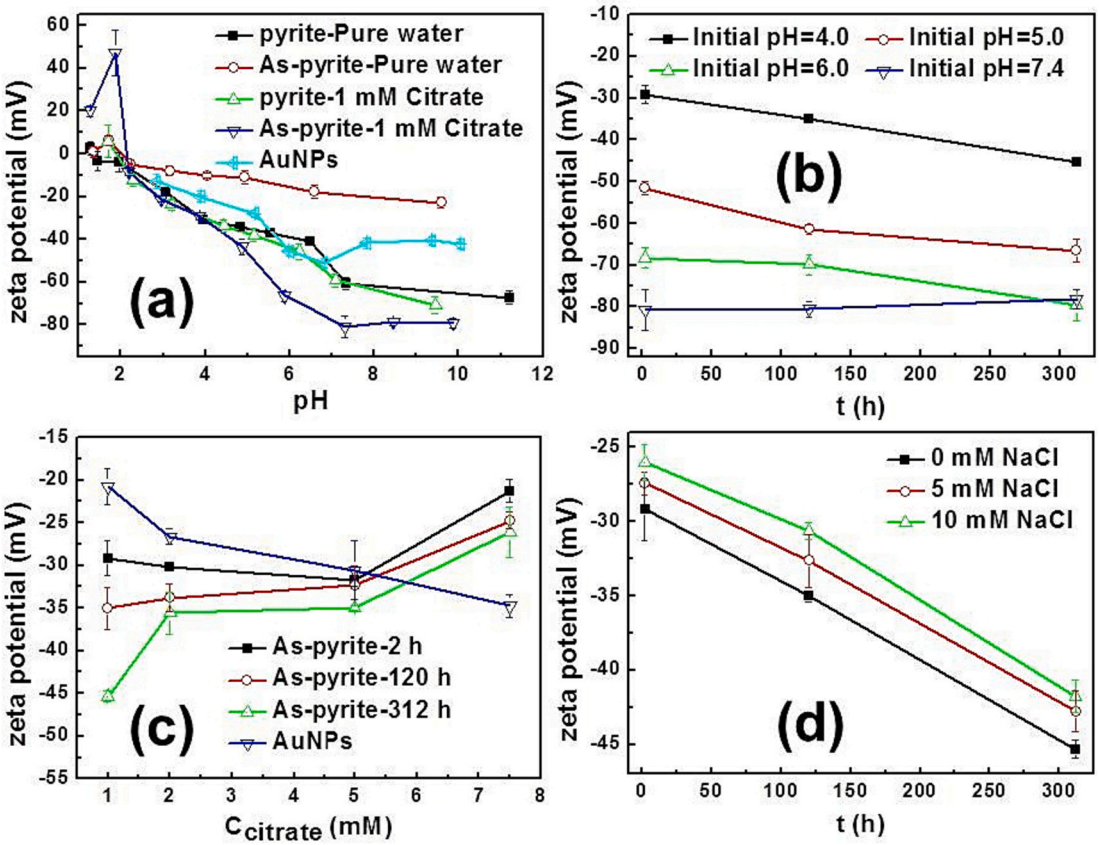

Fig. 6. Variations of zeta potentials of: (a) arsenian pyrite and pure pyrite in the absence or presence of citrate, and as-prepared AuNPs as a function of solution pH; (b) arsenian pyrite at different initial pHs in the presence of 1 mM citrate; (c) AuNPs and arsenian pyrite as a function of citrate concentration at initial pH 4.0; (d) arsenian pyrite with addition of different concentrations of NaCl in the presence of 1 mM citrate (initial pH 4.0).

credence to the aforementioned assumption that the citrate could interact with the surface of both arsenian pyrite and AuNPs. However, excessive citrate (7.5 mM) in the solution will increase the ionic strength, resulting in the decreased absolute zeta potential values of arsenian pyrite (Marzun et al., 2014). Furthermore, with increasing the stirring time, the zeta potential for arsenian pyrite would move toward a more negative direction, but the increased magnitude in the absolute value of zeta potential decreased with the increase of citrate concentration in the solution. The zeta potential of arsenian pyrite for citrate concentration of 1, 2, 5 and 7.5 mM was −45.33, −35.58, −35.01 and −26.14 mV at 312 h, respectively. This is presumably mainly due to the higher pH buffering capacity of higher concentration of citrate (Fig. 4b). This phenomenon further confirms that the citrate ligand plays multiple roles in the surface charge characteristics of arsenian pyrite.

Fig. 6d shows the variations of zeta potentials of arsenian pyrite with addition of different concentrations of NaCl solution. The zeta potential of arsenian pyrite became less negative with increasing ionic strength. On the other hand, the zeta potential of AuNPs showed no significant changes in response to an increase of ionic strength in this range (Supplemental Fig. S8).

4.2. Adsorption mechanism of AuNPs on arsenian pyrite

Based on the above results, it is shown once again that surface characteristics, especially surface charge characteristics, depend exquisitely on the chemical composition and atomic structure of the surface, the solution pH, and the solution chemical composition (in this case including citrate concentration and ionic strength). In this particular study, these surface and interface characteristics play crucial roles in the adsorption of AuNPs on arsenian pyrite. The cumulative effects of these physicochemical factors will determine the adsorption behavior of AuNPs in complex aqueous environments (Sharma et al., 2015; Wang et al., 2018). Although both arsenian pyrite and AuNPs are negatively charged over the pH range of this study, and are thereby expected to electrostatically repel each other, AuNPs can still be readily adsorbed on arsenian pyrite at certain pH values. Therefore, the existence of electrostatic attraction is not a necessary condition for the adsorption of AuNPs. Multiple interaction forces contribute to the adsorption mechanism of AuNPs and offset the electrostatic repulsions to a certain degree (Brittle et al., 2018; Fujita and Kobayashi, 2016).

It has been considered that the adsorption of AuNPs on arsenian pyrite are possibly dominated by bridging AuNPs and arsenian pyrite via citrate (Murphy and Strongin, 2009). A recognized explanation for the favorable attraction between like-charged substances (citrate and arsenian pyrite) is that a type of exceptionally strong hydrogen bonds (much stronger than ordinary hydrogen bonds), known as negative charge-assisted hydrogen bonds ((−)CAHBs), are formed between acidic oxyl/thiol groups on arsenian pyrite surfaces and carboxyl groups on citrate capping agents of AuNPs according to Eqs. (1)–(3) shown below (Ni and Pignatello, 2018; Uchimiya et al., 2017). The adsorption of citrate on arsenian pyrite according to Eqs. (1) and (3) will occur without the release of OH^-, while it will undergo release of OH^- in Eq. (2). (−)CAHBs possess a certain degree of covalent character, and in the limiting case makes it a 3-center, 4-electron covalent bond, which would reduce the reaction energy barrier between citrate and arsenian pyrite, thus facilitating the adsorption of citrate as well as AuNPs (Li et al., 2015; Ni et al., 2011).

$$-\mathrm{COOH} + {}^{-}\mathrm{O}/{}^{-}\mathrm{S}-\mathrm{pyrite} \rightarrow (-\mathrm{COO}\cdots\mathrm{H}\cdots\mathrm{O}/\mathrm{S}-\mathrm{pyrite})^{-} \quad (1)$$

$$-COO^- + H_2O + {}^-O/{}^-S - pyrite \rightarrow (-COO\cdots H\cdots O/S - pyrite)^- + OH^- \quad (2)$$

$$-COO^- + HO/HS - pyrite \rightarrow (-COO\cdots H\cdots O/S - pyrite)^- \quad (3)$$

To better understand the interaction mechanism between AuNPs and arsenian pyrite, the C 1 s XPS (Fig. 7a) and ATR-FTIR spectra (Fig. 7b) of the arsenian pyrite after adsorption of AuNPs were also measured. The spectrogram of C 1 s can be divided into three peaks. The peak at 284.6 eV can be assigned to adventitious carbon or internal standard carbon during XPS testing, or the C—C bond originated from citrate. And the peaks at 286.3 and 288.6 eV are identified as the bonds of C—O—H and C═O, respectively, corresponding to the hydroxyl and carboxyl groups of citrate (Liu et al., 2011; Mehtala and Wei, 2014). As shown in Fig. 7b, for the sample stirred in pure water for 312 h, only one characteristic FTIR peak at 433 cm^{-1} can be observed owing to the stretch of Fe^{2+}–$[S_2]^{2-}$ bonds. This is different from the standard spectrum of pyrite (407 cm^{-1}), suggesting that the incorporation of arsenic within the pyrite lattice could result in a peak shift to a higher wavenumber region (Sun et al., 2017). The band at 2360 cm^{-1} is attributed to absorbed CO_2 in air during ATR-FTIR testing. After adsorption of AuNPs, there are many new peaks at 3500, 1752, 1654, and 1430 cm^{-1} that are observed. The broad band near 3500 cm^{-1} is related to the stretching vibration of hydroxyl groups (–OH) which originated from –COOH or H_2O absorbed on the surface of samples (Nie et al., 2014). The peak at 1752 cm^{-1} represents C═O stretching vibration in the –COOH group. Specifically, the band observed at 1654 cm^{-1} might be ascribed to the stretching vibration of C═O groups in the (−)CAHBs of $(-COO\cdots H\cdots O/S - pyrite)^-$, in which the sharing of delocalized negative charges causes the equalization of electron density of C═O groups and the decrease of their bond force constants, and thus resulting in the reduced absorption frequency and the red-shifted stretching vibration from 1752 to 1654 cm^{-1}. The peak at 1431 cm^{-1} is attributable to the in-plane bending of –COH (Yang et al., 2017). These results confirm that the (−)CAHBs between citrate and arsenian pyrite might be the main interaction responsible for the adsorption of AuNPs onto arsenian pyrite.

According to extended DLVO (XDLVO) theory, the total potential energy, which is the sum of attractive (e.g., van der Waals attraction and (−)CAHBs between arsenian pyrite and AuNPs) and repulsive forces (e.g., electrostatic double layer (EDL) derived from charged surfaces of particles), should determine whether AuNPs can be adsorbed onto arsenian pyrite (Hotze et al., 2010; van Oss, 2003). When the attractive forces are greater than the repulsive forces, the adsorption of AuNPs on arsenian pyrite should occur. Such an adsorption process at favorable pH could be attributed to the synergistic effect between a multisite surface anchoring effect (formed through multiple (−)CAHBs) and van der Waals attraction (between arsenian pyrite and AuNPs). Fig. 8 demonstrates that the adsorbed citrate on arsenian pyrite can serve as anchoring units to link both AuNPs and arsenian pyrite via multiple (−)CAHBs, which efficiently enable AuNPs to anchor on arsenian pyrite surfaces by overcoming energy barriers (Al-Johani et al., 2017; Brittle et al., 2018; Park and Shumaker-Parry, 2014; Wang et al., 2015). The pseudo-zeroth-order kinetics also implies that the adsorption rate of AuNPs depends on the surface state of arsenian pyrite, i.e. available adsorption site density on arsenian pyrite surface as well as the contribution of (−)CAHBs between AuNPs and arsenian pyrite surfaces controlling the adsorption process (Jia et al., 2017; Yang et al., 2012b). As shown in Fig. 9, the schematic diagram of adsorption mechanisms for AuNPs on arsenian pyrite surface is proposed based on the above discussion. Overall, the combined effect of van der Waals attraction, (−)CAHBs, and electrostatic repulsion forces, which are influenced by the above-mentioned multiple factors, will determine the adsorption behavior of AuNPs on arsenian pyrite surface.

The surface structure of arsenian pyrite and AuNPs, including surface charge characteristics and types of surface functional groups, is critical to the adsorption process (Hotze et al., 2010; Mu et al., 2014; Yang et al., 2015). The decreased abundance of negatively charged thiol groups on arsenian pyrite surface leads to a less negative surface charge density compared with pure pyrite, and thus results in an obvious adsorption of AuNPs on arsenian pyrite surfaces rather than pure pyrite due to the decreased electrostatic repulsion between arsenian pyrite and AuNPs.

Nevertheless, (−)CAHBs are expected to be most energetically favorable at lower pH value (Li et al., 2015). Increasing pH enhances the EDL repulsion force between AuNPs and arsenian pyrite due to their increasing negative surface charge, suggesting that electrostatic interaction is a primary mechanism at higher pH (>6.0). At lower pH (4.0 and 5.0), the electrostatic repulsion between the relatively less negatively-charged surface of arsenian pyrite and AuNPs could be offset by attractive forces (van der Waals attraction and (−)CAHBs), which allows AuNPs to adsorb onto arsenian pyrite. Furthermore, the adsorbed AuNPs on arsenian pyrite will exert electrostatic repulsion to the suspended AuNPs in the solution to create a substantial energy barrier inhibiting further adsorption. This blocking effect is clearly supported by the observation that the adsorbed AuNPs on arsenian pyrite is well-separated and unagglomerated, and can be amplified at increased solution pH due to significantly increased negative charge on the surface of both AuNPs and arsenian pyrite (Fujita and Kobayashi, 2016; Luo et al., 2018).

Several mechanisms can elucidate the role of citrate during the adsorption of AuNPs on arsenian pyrite: (1) enhancing the negative surface charge of arsenian pyrite and AuNPs originating from higher citrate surface coverage; (2) competing for the adsorption sites with AuNPs; (3) serving as new adsorbing sites on arsenian pyrite surfaces which are beneficial to form (−)CAHBs between adsorbed citrate on arsenian pyrite and AuNPs; (4) offering more anchoring agents; (5) increasing the ionic strength of the solution; and (6) buffering the solution pH during the adsorption process (Uchimiya, 2014; Wang et al.,

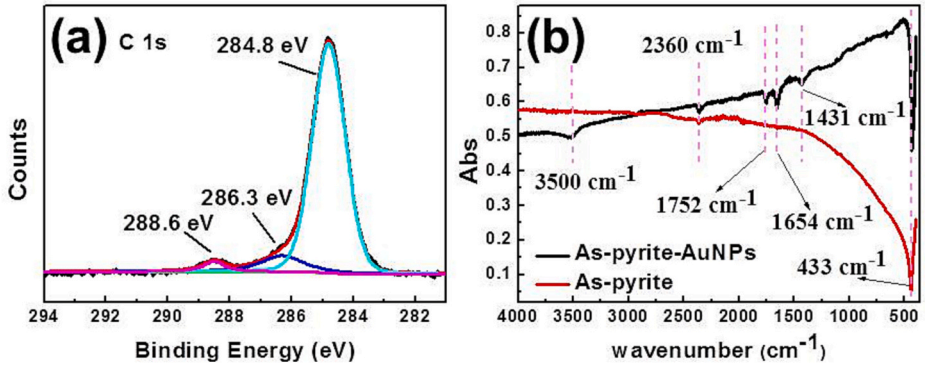

Fig. 7. (a) The C 1 s XPS of the arsenian pyrite after adsorption of AuNPs; (b) the attenuated total reflectance-Fourier transform infrared (ATR-FTIR) spectra of the arsenian pyrite after adsorption of AuNPs and stirred in pure water for 312 h.

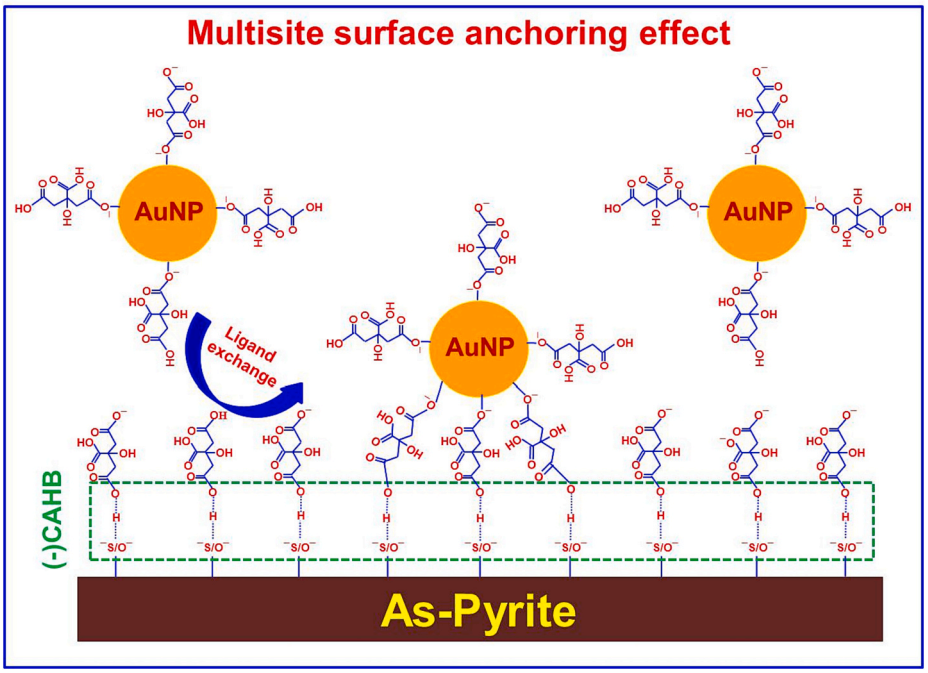

Fig. 8. Schematic diagram of multisite surface anchoring effect via negative charge–assisted hydrogen bonds.

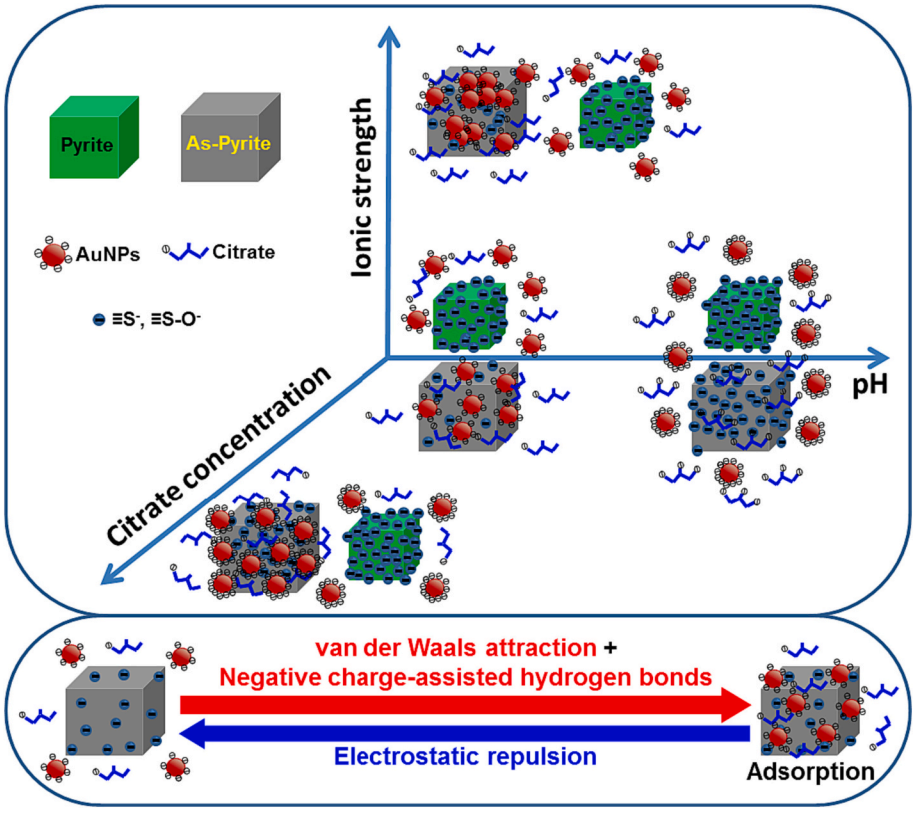

Fig. 9. Proposed schematic diagram of adsorption mechanisms for AuNPs on arsenian pyrite surface.

2015; Yang et al., 2012a). The mechanisms of (1)–(2) will impede the adsorption of AuNPs, while (3)–(6) will be conducive to the adsorption of AuNPs. Thus, the multiple interaction mechanisms, depending on the citrate concentration, ultimately modulate the surface charge and thus adsorption behavior of AuNPs by means of van der Waals interactions, electrostatic repulsion, and (−)CAHBs interactions (Gunsolus et al., 2015). The overall effect is that a higher citrate concentration could significantly enhance the adsorption rate of AuNPs.

Increasing ionic strength can reduce the zeta potential (consistent with Fig. 6d) and screen the repulsive forces owing to the decreased thickness of the electrostatic double layer. This results in the decrease of the maximum energy barrier of electrostatic repulsive forces between

negatively charged AuNPs and arsenian pyrite, which favors the adsorption of AuNPs (Atalay et al., 2014; Marzun et al., 2014; Tosco et al., 2012).

Based on direct spectral evidence (Fig. 7), we can unambiguously assert that the nature of surface sites of arsenian pyrite and the solution chemistry (especially pH) are primary factors governing the adsorption behavior of AuNPs. Desorption experiment was conducted by stirring arsenian pyrite separated from sorption suspension. No AuNPs were detected in the supernatant after stirring the arsenian pyrite adsorbed with AuNPs for up to 17 days in a solution containing 1 mM citrate at pH 4.0. SEM images (Supplemental Fig. S9) indicate that most AuNPs were still adsorbed on the surface of arsenian pyrite. The result suggests that a small amount of surface-bound citrate on AuNPs could form strong (−) CAHBs with the surface functional groups on the arsenian pyrite, which may induce irreversible adsorption of AuNPs.

4.3. Geochemical implications

Aqueous complexations (e.g. hydrosulphide and chloride complexes) have long been considered as the predominant transported species of gold in hydrothermal systems. However, this hypothesis cannot readily explain the formation of some ultrahigh-grade gold deposits by the exceptionally low solubility of gold (ppb level) as aqueous complexations in hydrothermal fluids, and consequently, an alternative gold transport mechanism is needed (Liu et al., 2019; McLeish et al., 2021; Petrella et al., 2022). Several recent studies provided indirect and direct evidence for the existence of gold nanoparticles (or colloidal gold particles) in hydrothermal fluids and many gold deposit types, indicating that AuNPs may play an important role in transporting and/or accumulating processes responsible for forming gold deposits (Gartman et al., 2019; Gartman et al., 2017; Hannington and Garbe-Schonberg, 2019; Hannington et al., 2016; Liu et al., 2019; McLeish et al., 2021; Petrella et al., 2020). Thus, a complete gold transport model in active geothermal systems should include both dissolved and particulate gold species. AuNPs or colloids with negative surface charge could be formed in the deeper parts of hydrothermal systems and indefinitely transported in a hydrothermal fluid phase in a natural system due to larger net repulsive forces than net attractive forces (Hastie et al., 2021; McLeish et al., 2021; Saunders, 1990; Williams-Jones et al., 2009). The transport and deposition mechanisms of AuNPs should be significantly different from the aqueous gold complexations in hydrothermal fluids. The transport of gold in the form of nanoparticles with higher gold content is more efficient than their transport in aqueous complexations in aqueous solutions, which may explain the origin of high-grade gold ores (Petrella et al., 2022; Saunders, 1990).

The transport, aggregation, and deposition of AuNPs to form much larger Au masses may also be an important intermediary step in forming high-grade gold deposits through changes in liquid phase conditions, including pH, temperature, pressure or solution chemistry, and adsorption via physical interaction with specific mineral surfaces (Fougerouse et al., 2016; Hannington et al., 2016; Hough et al., 2011; McLeish et al., 2021; Petrella et al., 2022; Saunders et al., 2020; Williams-Jones et al., 2009). For example, it has been suggested that moderately acidic ore fluids (pH ~ 4–6) are more favorable for the precipitation of Au in arsenian pyrite in hydrothermal systems (Cline, 2018; Hannington et al., 2016; Hu et al., 2002; Xie et al., 2017), which coincides with our results that the adsorption and deposition of negatively charged AuNPs on arsenian pyrite surfaces only occurs at pH < 6. Furthermore, when AuNPs are mechanically transported in hydrothermal fluid mixed with high salinity seawater, they would be flocculated and ultimately formed localized hyperenrichments of gold in the deposit (McLeish et al., 2021).

Sulfide minerals (particularly arsenian pyrite) are important minerals in ores of magmatic, hydrothermal, and supergene origin. Au could exist in these minerals mainly in the “invisible” state, including nanoscale particles and/or chemically bound Au; a positive correlation between Au and As concentrations is observed (Deditius et al., 2014; Reich et al., 2005). Our work suggests that AuNPs are preferentially enriched on arsenian pyrite surfaces instead of pure pyrite via adsorption, which validates that arsenian pyrite acts as one of the major phases controlling Au enrichment. Although many studies (all referenced here) show that invisible Au may occur primarily as ionically bonded Au in arsenian pyrite and AuNPs might be formed through subsequent metamorphic or weathering processes, our findings could also be used to explain that the enrichment of Au(I) complexes may also be initially controlled by surface properties, especially surface charge characteristics of arsenian pyrite. Abundant crystal surface and bulk defects, originating from the incorporation of As, would also facilitate the adsorbed Au which is incorporated into the growing arsenian pyrite lattice, leading to a coupled geochemistry of Au and As in pyrite from various hydrothermal ore deposits (Kusebauch et al., 2019; Wu et al., 2021).

In addition, numerous metal nanoparticles can be formed by natural or manufacturing processes in various environments, including aerosols, waters, soil, and microbial systems. These metal nanoparticles could interact with various materials during transport processes, which ultimately changes their transport and fate. Their cycle in various Earth compartments also plays a crucial role in many geochemical processes (Sharma et al., 2015). Our results indicate that the surface charge properties of AuNPs and arsenian pyrite, which are partly controlled by the solution properties, are largely responsible for the selective adsorption behavior of AuNPs on arsenian pyrite, implying the high complexity of the adsorption behaviors for metal nanoparticles on mineral surfaces. The combined effects of various physicochemical factors, including solid phase structure, pH, concentration and nature of natural organic matter, ionic strength, ionic components, redox conditions, will determine the aggregation, transport, and deposition of metal nanoparticles.

Moreover, in Earth’s surface environment and many types of hydrothermal ore deposits, organic matter (e.g. humic substances) is a ubiquitous and abundant constituent with concentrations ranging from sub mg/L levels to tens of mg/L, which is stable and can form complexes with Au via carboxyl (–COOH), hydroxyl (–OH), and thiol (–SH) groups, and consequently will play a key role in the formation, transport and fate of AuNPs (Crede et al., 2019; Hu et al., 2002; Sharma et al., 2015). AuNPs could be typically stabilized and transported by various organic matter, such as humic substances, saccharides, surfactants and polymers (Saunders, 1990; Sharma et al., 2015). Our findings indicate that a higher citrate concentration could significantly enhance the adsorption rate of AuNPs due to the formation of (−)CAHBs between the surface of arsenian pyrite and citrate-capped AuNPs. The citrate-caped AuNPs solutions are stable up to 225 °C, implying that natural organic matter may contribute to gold transport in various low-temperature hydrothermal systems and supergene environments and have an active role in influencing the geochemical behavior of AuNPs (Crede et al., 2019; Liu et al., 2019). Because the carboxyl groups of natural organic matter have similar functions as on citrate, they would also very likely form strong (−)CAHBs with specific mineral surfaces under certain conditions, leading to the aggregation and deposition of AuNPs.

In terms of the fate of AuNPs, several environmental factors determine their transport and deposition in the complex environmental matrices. It should be emphasized that the investigation of the transport, fate, and reactivity for metal nanoparticles at elevated temperature and pressure typical of near-surface to deep-crustal conditions is rare up to now. More parameters should be taken into account for elucidating the interaction mechanisms between metal nanoparticles and minerals under hydrothermal condition, and thus further investigation should be performed for better understanding the transport and deposition mechanisms of AuNPs. Even so, our study should help in the understanding and prediction of nanoparticle-mineral interface interactions as well as their related geochemical behavior in hydrothermal systems and Earth’s surface environment.

5. Conclusions

The adsorption behaviors of negatively charged AuNPs on synthetic pyrite and arsenian pyrite were comparatively conducted under an anaerobic condition. Negligible adsorption of AuNPs on pure pyrite surface was observed under all experimental conditions. AuNPs could be preferentially adsorbed on arsenian pyrite surface probably due to the formation of strong negative charge–assisted hydrogen bonds between hydroxyl/oxyl groups on the surface of arsenian pyrite and carboxyl groups on citrate capping agents of AuNPs. The solution pH, coexisting organics (citrate) concentration, and ionic strength are likely controls for the adsorption processes of AuNPs on arsenian pyrite. The combined effect of van der Waals attraction, negative charge-assisted hydrogen bonds, and electrostatic repulsion forces, controls the adsorption behavior of AuNPs on arsenian pyrite surface. These results imply that AuNPs may be an important transport mechanism for gold in hydrothermal systems, and their subsequent flocculated aggregation and deposition with arsenian pyrite may help explain the accumulating processes contributing to the eventual formation of "invisible" gold in sulfide minerals in many high-grade hydrothermal gold deposits. The adsorption and deposition of AuNPs on arsenian pyrite surface not only may be an important intermediary step in forming high-grade gold deposits, but may also have strong influence on the environmental fate and transport of AuNPs in the Earth's surface environment, which will affect the bioavailability as well as toxicity of AuNPs on ecosystem and human health. These findings will help to comprehensively explain the interaction mechanism between AuNPs and arsenian pyrite, and can also provide new insights for understanding the transport and deposition mechanism of gold nanoparticles in the hydrothermal systems and assessing the environmental behavior of gold nanoparticles in the Earth's surface environment.

Declaration of Competing Interest

The authors declare that they have no known competing financial interests or personal relationships that could have appeared to influence the work reported in this paper.

Data availability

Data will be made available on request.

Acknowledgments

This work was financially supported by the B-type Strategic Priority Program of the Chinese Academy of Sciences (XDB41000000), the National Natural Science Foundation of China (41902041, 41872046), the Guizhou Provincial Science and Technology Projects ([2018]1172, [2020]1Z039), and the Opening Fund of State Key Laboratory of Ore Deposit Geochemistry (201602).

Appendix A. Supplementary data

Supplementary data to this article can be found online at https://doi.org/10.1016/j.chemgeo.2023.121747.

References

Abraitis, P.K., Pattrick, R.A.D., Vaughan, D.J., 2004. Variations in the compositional, textural and electrical properties of natural pyrite: a review. Int. J. Miner. Process. 74, 41–59.
Al-Johani, H., Abou-Hamad, E., Jedidi, A., Widdifield, C.M., Viger-Gravel, J., Sangaru, S. S., Gajan, D., Anjum, D.H., Ould-Chikh, S., Hedhili, M.N., Gurinov, A., Kelly, M.J., El Eter, M., Cavallo, L., Emsley, L., Basset, J.M., 2017. The structure and binding mode of citrate in the stabilization of gold nanoparticles. Nat. Chem. 9, 890–895.
Atalay, S., Ma, Y., Qian, S.Z., 2014. Analytical model for charge properties of silica particles. J. Colloid Interface Sci. 425, 128–130.
Bebie, J., Schoonen, M.A.A., Fuhrmann, M., Strongin, D.R., 1998. Surface charge development on transition metal sulfides: an electrokinetic study. Geochim. Cosmochim. Ac 62, 633–642.
Beck, M.T., 1977. Critical evaluation of equilibrium-constants in solution stability-constants of metal-complexes. Pure Appl. Chem. 49, 129–135.
Becker, U., Reich, M., Biswas, S., 2010. Nanoparticle-host interactions in natural systems, nanoscopic approaches in Earth and planetary sciences. EMU Notes Mineral. 1–52.
Blanchard, M., Alfredsson, M., Brodholt, J., Wright, K., Catlow, C.R.A., 2007. Arsenic incorporation into FeS_2 pyrite and its influence on dissolution: a DFT study. Geochim. Cosmochim. Ac 71, 624–630.
Brittle, S.W., Foose, D.P., O'Neil, K.A., Sikon, J.M., Johnson, J.K., Stahler, A.C., Ryan, J., Higgins, S.R., Sizemore, I.E., 2018. A Raman-based imaging method for characterizing the molecular adsorption and spatial distribution of silver nanoparticles on hydrated mineral surfaces. Environ. Sci. Technol. 52, 2854–2862.
Cline, J.S., 2018. Diversity of Carlin-style gold deposits. In: Muntean, J.L. (Ed.), Reviews in Economic Geology. Society of Economic Geologists, Inc., pp. 7–38
Crede, L.S., Liu, W.H., Evans, K.A., Rempel, K.U., Testemale, D., Brugger, J., 2019. Crude oils as ore fluids: an experimental in-situ XAS study of gold partitioning between brine and organic fluid from 25 to 250 degrees C. Geochim. Cosmochim. Ac 244, 352–365.
Deditius, A.P., Utsunomiya, S., Renock, D., Ewing, R.C., Ramana, C.V., Becker, U., Kesler, S.E., 2008. A proposed new type of arsenian pyrite: composition, nanostructure and geological significance. Geochim. Cosmochim. Ac 72, 2919–2933.
Deditius, A.P., Reich, M., Kesler, S.E., Utsunomiya, S., Chryssoulis, S.L., Walshe, J., Ewing, R.C., 2014. The coupled geochemistry of Au and As in pyrite from hydrothermal ore deposits. Geochim. Cosmochim. Ac 140, 644–670.
Fougerouse, D., Reddy, S.M., Saxey, D.W., Rickard, W.D.A., van Riessen, A., Micklethwaite, S., 2016. Nanoscale gold clusters in arsenopyrite controlled by growth rate not concentration: evidence from atom probe microscopy. Am. Mineral. 101, 1916–1919.
Fu, Y.H., Nie, X., Qin, Z.H., Li, S.S., Wan, Q., 2017. Effect of particle size and pyrite oxidation on the sorption of gold nanoparticles on the surface of pyrite. J. Nanosci. Nanotechnol. 17, 6367–6376.
Fujita, Y., Kobayashi, M., 2016. Transport of colloidal silica in unsaturated sand: effect of charging properties of sand and silica particles. Chemosphere 154, 179–186.
Gartman, A., Hannington, M., Jamieson, J.W., Peterkin, B., Garbe-Schönberg, D., Findlay, A.J., Fuchs, S., Kwasnitschka, T., 2017. Boiling-induced formation of colloidal gold in black smoker hydrothermal fluids. Geology 46, 39–42.
Gartman, A., Findlay, A.J., Hannington, M., Garbe-Schonberg, D., Jamieson, J.W., Kwasnitschka, T., 2019. The role of nanoparticles in mediating element deposition and transport at hydrothermal vents. Geochim. Cosmochim. Ac 261, 113–131.
Gong, M.G., Kirkeminde, A., Kumar, N., Zhao, H., Ren, S.Q., 2013. Ionic-passivated FeS_2 photocapacitors for energy conversion and storage. Chem. Commun. 49, 9260–9262.
Gopon, P., Douglas, J.O., Auger, M.A., Hansen, L., Wade, J., Cline, J.S., Robb, L.J., Moody, M.P., 2019. A Nanoscale Investigation of Carlin-Type Gold deposits: An Atom-Scale Elemental and Isotopic Perspective. Econ. Geol. 114, 1123–1133.
Gunsolus, I.L., Mousavi, M.P.S., Hussein, K., Buhlmann, P., Haynes, C.L., 2015. Effects of humic and fulvic acids on silver nanoparticle stability, dissolution, and toxicity. Environ. Sci. Technol. 49, 8078–8086.
Hannington, M., Garbe-Schonberg, D., 2019. Detection of gold nanoparticles in hydrothermal fluids. Econ. Geol. 114, 397–400.
Hannington, M., Haroardottir, V., Garbe-Schonberg, D., Brown, K.L., 2016. Gold enrichment in active geothermal systems by accumulating colloidal suspensions. Nat. Geosci. 9, 299–302.
Hastie, E.C.G., Schindler, M., Kontak, D.J., Lafrance, B., 2021. Transport and coarsening of gold nanoparticles in an orogenic deposit by dissolution–reprecipitation and Ostwald ripening. Commun. Earth Environ. 2, 57.
Hochella, M.F., Mogk, D.W., Ranville, J., Allen, I.C., Luther, G.W., Marr, L.C., McGrail, B. P., Murayama, M., Qafoku, N.P., Rosso, K.M., Sahai, N., Schroeder, P.A., Vikesland, P., Westerhoff, P., Yang, Y., 2019. Natural, incidental, and engineered nanomaterials and their impacts on the Earth system. Science 363, 1414.
Hotze, E.M., Phenrat, T., Lowry, G.V., 2010. Nanoparticle aggregation: challenges to understanding transport and reactivity in the environment. J. Environ. Qual. 39, 1909–1924.
Hough, R.M., Noble, R.R.P., Reich, M., 2011. Natural gold nanoparticles. Ore Geol. Rev. 42, 55–61.
Hu, R.Z., Su, W.C., Bi, X.W., Tu, G.Z., Hofstra, A.H., 2002. Geology and geochemistry of Carlin-type gold deposits in China. Mineral. Deposita 37, 378–392.
Jia, Y.Y., Khanal, S.K., Zhang, H.Q., Chen, G.H., Lu, H., 2017. Sulfamethoxazole degradation in anaerobic sulfate-reducing bacteria sludge system. Water Res. 119, 12–20.
Kusebauch, C., Gleeson, S.A., Oelze, M., 2019. Coupled partitioning of Au and As into pyrite controls formation of giant Au deposits. Sci. Adv. 5.
Large, R.R., Danyushevsky, L., Hollit, C., Maslennikov, V., Meffre, S., Gilbert, S., Bull, S., Scott, R., Emsbo, P., Thomas, H., Singh, B., Foster, J., 2009. Gold and trace element zonation in pyrite using a laser imaging technique: implications for the timing of gold in orogenic and Carlin-style sediment-hosted deposits. Econ. Geol. 104, 635–668.
Le Pape, P., Blanchard, M., Brest, J., Boulliard, J.C., Ikogou, M., Stetten, L., Wang, S., Landrot, G., Morin, G., 2017. Arsenic incorporation in pyrite at ambient temperature at both Tetrahedral S-I and Octahedral Fe-II Sites: evidence from EXAFS-DFT analysis. Environ. Sci. Technol. 51, 150–158.
Lee, S., Xu, H., Wempner, J., Xu, H., Wen, J., 2021. Discovery of gold nanoparticles in Marcellus Shale. ACS Earth Space Chem. 5, 129–135.

Li, X.Y., Gamiz, B., Wang, Y.Q., Pignatello, J.J., Xing, B.S., 2015. Competitive sorption used to probe strong hydrogen bonding sites for weak organic acids on carbon nanotubes. Environ. Sci. Technol. 49, 1409–1417.
Liu, H.B., Wu, Y.M., Zhang, J.L., 2011. A new approach toward carbon-modified vanadium-doped titanium dioxide photocatalysts. ACS Appl. Mater. Interfaces 3, 1757–1764.
Liu, W.H., Chen, M., Yang, Y., Mei, Y., Etschmann, B., Brugger, J., Johannessen, B., 2019. Colloidal gold in Sulphur and citrate-bearing hydrothermal fluids: an experimental study. Ore Geol. Rev. 114.
Luo, S., Nie, X., Yang, M., Fu, Y., Zeng, P., Wan, Q., 2018. Sorption of differently charged gold nanoparticles on synthetic pyrite. Minerals 8, 428.
Marzun, G., Streich, C., Jendrzej, S., Barcikowski, S., Wagener, P., 2014. Adsorption of colloidal platinum nanoparticles to supports: charge transfer and effects of electrostatic and steric interactions. Langmuir 30, 11928–11936.
McLeish, D.F., Williams-Jones, A.E., Vasyukova, O.V., Clark, J.R., Board, W.S., 2021. Colloidal transport and flocculation are the cause of the hyperenrichment of gold in nature. P. Natl. Acad. Sci. USA 118, e2100689118.
Mehtala, J.G., Wei, A., 2014. Nanometric resolution in the hydrodynamic size analysis of ligand-stabilized gold nanorods. Langmuir 30, 13737–13743.
Migdisov, A.A., Guo, X., Xu, H., Williams-Jones, A.E., Sun, C.J., Vasyukova, O., Sugiyama, I., Fuchs, S., Pearce, K., Roback, R., 2017. Hydrocarbons as ore fluids. Geochem. Perspect. Lett. 5, 47–52.
Mikhlin, Y.L., Romanchenko, A.S., Asanov, I.P., 2006. Oxidation of arsenopyrite and deposition of gold on the oxidized surfaces: a scanning probe microscopy, tunneling spectroscopy and XPS study. Geochim. Cosmochim. Ac 70, 4874–4888.
Mikhlin, Y., Romanchenko, A., Likhatski, M., Karacharov, A., Erenburg, S., Trubina, S., 2011. Understanding the initial stages of precious metals precipitation: Nanoscale metallic and sulfidic species of gold and silver on pyrite surfaces. Ore Geol. Rev. 42, 47–54.
Miller, M.R., Raftis, J.B., Langrish, J.P., McLean, S.G., Samutrtai, P., Connell, S.P., Wilson, S., Vesey, A.T., Fokkens, P.H.B., Boere, A.J.F., Krystek, P., Campbell, C.J., Hadoke, P.W.F., Donaldson, K., Cassee, F.R., Newby, D.E., Duffin, R., Mills, N.L., 2017. Inhaled nanoparticles accumulate at sites of vascular disease. ACS Nano 11, 4542–4552.
Mu, Q.X., Jiang, G.B., Chen, L.X., Zhou, H.Y., Fourches, D., Tropsha, A., Yan, B., 2014. Chemical basis of interactions between engineered nanoparticles and biological systems. Chem. Rev. 114, 7740–7781.
Murphy, R., Strongin, D.R., 2009. Surface reactivity of pyrite and related sulfides. Surf. Sci. Rep. 64, 1–45.
Nesbitt, H.W., Bancroft, G.M., Pratt, A.R., Scaini, M.J., 1998. Sulfur and iron surface states on fractured pyrite surfaces. Am. Mineral. 83, 1067–1076.
Ni, J.Z., Pignatello, J.J., 2018. Charge-assisted hydrogen bonding as a cohesive force in soil organic matter: water solubility enhancement by addition of simple carboxylic acids. Environ. Sci. Proc. Imp. 20, 1225–1233.
Ni, J.Z., Pignatello, J.J., Xing, B.S., 2011. Adsorption of aromatic carboxylate ions to black carbon (biochar) is accompanied by proton exchange with water. Environ. Sci. Technol. 45, 9240–9248.
Nie, X., Li, G.Y., Wong, P.K., Zhao, H.J., An, T.C., 2014. Synthesis and characterization of N-doped carbonaceous/TiO_2 composite photoanodes for visible-light photoelectrocatalytic inactivation of *Escherichia coli* K-12. Catal. Today 230, 67–73.
Nie, X., Li, G., Li, S., Luo, Y., Luo, W., Wan, Q., An, T., 2022. Highly efficient adsorption and catalytic degradation of ciprofloxacin by a novel heterogeneous Fenton catalyst of hexapod-like pyrite nanosheets mineral clusters. Appl. Catal. B Environ. 300, 120734.
Park, J.W., Shumaker-Parry, J.S., 2014. Structural study of citrate layers on gold nanoparticles: role of intermolecular interactions in stabilizing nanoparticles. J. Am. Chem. Soc. 136, 1907–1921.
Park, J.W., Shumaker-Parry, J.S., 2015. Strong resistance of citrate anions on metal nanoparticles to desorption under thiol functionalization. ACS Nano 9, 1665–1682.
Petrella, L., Thebaud, N., Fougerouse, D., Evans, K., Quadir, Z., Laflamme, C., 2020. Colloidal gold transport: a key to high-grade gold mineralization? Mineral. Deposita 55, 1247–1254.
Petrella, L., Thebaud, N., Fougerouse, D., Tattitch, B., Martin, L., Turner, S., Suvorova, A., Gain, S., 2022. Nanoparticle suspensions from carbon-rich fluid make high-grade gold deposits. Nat. Commun. 13, 3795.
Pokrovski, G.S., Escoda, C., Blanchard, M., Testemale, D., Hazemann, J.L., Gouy, S., Kokh, M.A., Boiron, M.C., Parseval, F.d., Aigouy, T., Menjot, L., Parseval, P.d., Proux, O., Rovezzi, M., Béziat, D., Salvi, S., Kouzmanov, K., Bartsch, T., Pöttgen, R., Doert, T., 2021. An arsenic-driven pump for invisible gold in hydrothermal systems. Geochem. Perspect. Lett. 17, 39–44.
Qiu, G.H., Gao, T.Y., Hong, J., Luo, Y., Liu, L.H., Tan, W.F., Liu, F., 2018. Mechanisms of interaction between arsenian pyrite and aqueous arsenite under anoxic and oxic conditions. Geochim. Cosmochim. Ac 228, 205–219.
Reich, M., Kesler, S.E., Utsunomiya, S., Palenik, C.S., Chryssoulis, S.L., Ewing, R.C., 2005. Solubility of gold in arsenian pyrite. Geochim. Cosmochim. Ac 69, 2781–2796.
Reich, M., Hough, R.M., Deditius, A., Utsunomiya, S., Ciobanu, C.L., Cook, N.J., 2011. Nanogeoscience in ore systems research: principles, methods, and applications introduction and preface to the special issue preface. Ore Geol. Rev. 42, 1–5.
Saunders, J.A., 1990. Colloidal transport of gold and silica in epithermal precious-metal systems - evidence from the sleeper deposit, Nevada. Geology 18, 757–760.
Saunders, J.A., Burke, M., Brueseke, M.E., 2020. Scanning-electron-microscope imaging of gold (electrum) nanoparticles in middle Miocene bonanza epithermal ores from northern Nevada, USA. Mineral. Deposita 55, 389–398.
Sharma, V.K., Siskova, K.M., Zboril, R., Gardea-Torresdey, J.L., 2014. Organic-coated silver nanoparticles in biological and environmental conditions: fate, stability and toxicity. Adv. Coll. Interfac. 204, 15–34.
Sharma, V.K., Filip, J., Zboril, R., Varma, R.S., 2015. Natural inorganic nanoparticles - formation, fate, and toxicity in the environment. Chem. Soc. Rev. 44, 8410–8423.
Sun, Y., Lv, D., Zhou, J.S., Zhou, X.X., Lou, Z.M., Baig, S.A., Xu, X.H., 2017. Adsorption of mercury (II) from aqueous solutions using FeS and pyrite: a comparative study. Chemosphere 185, 452–461.
Thiel, J., Byrne, J.M., Kappler, A., Schink, B., Pester, M., 2019. Pyrite formation from FeS and H_2S is mediated through microbial redox activity. P. Natl. Acad. Sci. USA 116, 6897–6902.
Tosco, T., Bosch, J., Meckenstock, R.U., Sethi, R., 2012. Transport of Ferrihydrite Nanoparticles in Saturated Porous Media: Role of Ionic Strength and Flow Rate. Environ. Sci. Technol. 46, 4008–4015.
Uchimiya, S., 2014. Influence of pH, ionic strength, and multidentate ligand on the interaction of CdII with biochars. ACS Sustain. Chem. Eng. 2, 2019–2027.
Uchimiya, M., Pignatello, J.J., White, J.C., Hu, S.L., Ferreira, P.J., 2017. Surface interactions between gold nanoparticles and biochar. Sci. Rep. UK 7.
van Oss, C.J., 2003. Long-range and short-range mechanisms of hydrophobic attraction and hydrophilic repulsion in specific and aspecific interactions. J. Mol. Recognit. 16, 177–190.
Wang, H.Y., Jia, H.R., Lu, X.L., Chen, B., Zhou, G.X., He, N.Y., Chen, Z., Wu, F.G., 2015. Imaging plasma membranes without cellular internalization: multisite membrane anchoring reagents based on glycol chitosan derivatives. J. Mater. Chem. B 3, 6165–6173.
Wang, X.Z., Adeleye, A.S., Wang, H.H., Zhang, M., Liu, M.M., Wang, Y.Y., Li, Y., Keller, A.A., 2018. Interactions between polybrominated diphenyl ethers (PBDEs) and TiO_2 nanoparticle in artificial and natural waters. Water Res. 146, 98–108.
Weerasooriya, R., Tobschall, H.J., 2005. Pyrite-water interactions: effects of pH and pFe on surface charge. Coll. Surf. A 264, 68–74.
Wen, X., Wei, X.L., Yang, L.W., Shen, P.K., 2015. Self-assembled FeS_2 cubes anchored on reduced graphene oxide as an anode material for lithium ion batteries. J. Mater. Chem. A 3, 2090–2096.
Williams-Jones, A.E., Bowell, R.J., Migdisov, A.A., 2009. Gold in solution. Elements 5, 281–287.
Wu, Y.F., Evans, K., Hu, S.Y., Fougerouse, D., Zhou, M.F., Fisher, L.A., Guagliardo, P., Li, J.W., 2021. Decoupling of Au and As during rapid pyrite crystallization. Geology. 49, 827–831.
Xian, H., He, H., Zhu, J., Qiu, K., Li, Y., Yang, Y., Xing, J., Tan, W., Tsuchiyama, A., Yastake, M., Enju, S., Miyake, A., Zhu, R., 2022. Hyperenrichment of gold in pyrite induced by solid-state transportation. Commun. Earth Environ. 3, 308.
Xie, Z.J., Xia, Y., Cline, J.S., Yan, B.W., Wang, Z.P., Tan, Q.P., Wei, D.T., 2017. Comparison of the native antimony-bearing Paiting gold deposit, Guizhou Province, China, with Carlin-type gold deposits, Nevada, USA. Mineral. Deposita 52, 69–84.
Yang, H.Y., Kim, H., Tong, M.P., 2012a. Influence of humic acid on the transport behavior of bacteria in quartz sand. Coll. Surf. B 91, 122–129.
Yang, S.F., Lin, C.F., Wu, C.J., Ng, K.K., Lin, A.Y.C., Hong, P.K.A., 2012b. Fate of sulfonamide antibiotics in contact with activated sludge - sorption and biodegradation. Water Res. 46, 1301–1308.
Yang, C., Xie, H., Li, Q.C., Sun, E.J., Su, B.L., 2015. Adherence and interaction of cationic quantum dots on bacterial surfaces. J. Colloid Interface Sci. 450, 388–395.
Yang, W., Wang, Y., Sharma, P., Li, B.G., Liu, K.S., Liu, J., Flury, M., Shang, J.Y., 2017. Effect of naphthalene on transport and retention of biochar colloids through saturated porous media. Coll. Surf. A 530, 146–154.
Zhou, H.Y., Wirth, R., Gleeson, S.A., Schreiber, A., Mayanna, S., 2021. Three-dimensional and microstructural fingerprinting of gold nanoparticles at fluid-mineral interfaces. Am. Mineral. 106, 97–104.
Zhu, J.X., Xian, H.Y., Lin, X.J., Tang, H.M., Du, R.X., Yang, Y.P., Zhu, R.L., Liang, X.L., Wei, J.M., Teng, H.H., He, H.P., 2018. Surface structure-dependent pyrite oxidation in relatively dry and moist air: Implications for the reaction mechanism and sulfur evolution. Geochim. Cosmochim. Ac 228, 259–274.